Aerodynamic tunnel trials in order to apply active aerodynamic contrtol to a high speed train

Pedro Miguel dos Santos Fernandes
pedro.s.fernandes@tecnico.ulisboa.pt

Instituto Superior Técnico, Universidade de Lisboa, Portugal

November 2017

Abstract

This study focuses on the aerodynamic performance of a particular compact lightweight high-speed train, having a very streamlined surface. The three-dimensional geometry of the train, as well as the asymmetry of the impinging relative flow due to lateral wind, twist the boundary layer and may lead to separation and the appearance of longitudinal vortices. These vortices change the pressure distribution, resulting in aerodynamic forces (e.g. with lateral, vertical and drag components), instability and noise. In order to minimize or inhibit boundary layer twisting, it is of interest to use the suction boundary layer technique in which, through small holes or grooves in the surface, air is drawn from the boundary layer. As a first step to apply this technique, the boundary layer was experimentally studied. To do so, a 1:10 scale model was built. Oil film visualization was applied. That technique was developed to understand the physical mechanism of formation of streaklines over the solid surface, that render the direction of the limiting lines. The model was tested in wind tunnel to identify the boundary layer twist and the convergence of surface streamlines, related with flow separation. The streaklines pattern, was helpful to suggest areas where it would be useful to extract the low velocity fluid from the boundary layer. The ultimate goal will be to eliminate the inception of longitudinal vortices to improve the symmetry of the pressure distribution, contributing to greater stability and safety, as well as a reduction in aerodynamic drag.

Keywords: Suction control, boundary layer, flow control, compact lightweight high-speed train, longitudinal vortices, oil-film visualizations

1. Introduction

Growing concerns about the energy efficiency, comfort and safety of rail vehicles motivate the control of the boundary layer, namely its twisting, responsible for the formation of longitudinal vortices. The delay or even the inhibition of boundary layer separation allows better control of the formation of these vortices, and thereby also controlling the pressure distribution on the surface of the vehicle, which in the present case is a high-speed light train.

The control is done using the suction technique, where, through strategically placed small holes or grooves, the extraction of fluid with a low amount of movement is sought, avoiding the convergence of surface current lines and three-dimensional separation.

The amount of fluid withdrawn from the surface is small relative to the amount of fluid flowing around the vehicle, which makes it possible to control suction, with the possibility of conducting the extracted air inside the fuselage to later inject it into another passable zone separation - blow control - as suggested in [1].

In this way, aerodynamic forces can be reduced, contributing to greater vehicle stability, insofar as the risk of lateral collapse is minimized. The noise generation is also reduced since this has mainly origin in the longitudinal vortices and in the instabilities of the boundary layer in the side wall.

2. Compact lightweight high-speed train

The geometry of the train consists of a fuselage body, with 18 m in length and a capacity of 40 seats. Although in the prototype there are accessories that aim at aerodynamic optimization, such as wheel fairing, they do not exist in the model. The same represents only the fuselage geometry of the prototype, therefore a non-detailed version of the same. The measurements of the model are represented in the figure 1. A number of other advantages are also mentioned, such as the reduced cross-sectional area, which reduces the blocking effect in tunnels, thus reducing the pressure wavefront formed at the entrance of the tunnels, and the geo-

metric configuration that shows benefits at the level of the structural and dynamic behaviour of the train [7]. The ease of applying certain boundary layer control techniques, such as suction and blowing, is also an advantage of the short train, as suggested in [1].

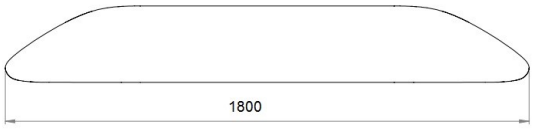

(a) Length

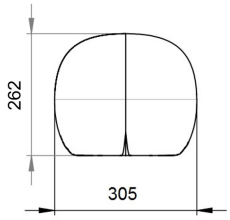

(b) Width and height

Figure 1: Dimensions, in *mm*, of the 1:10 scale model.

3. Boundary Layer Control

Longitudinal vortices Issues related to train stability and safety are intrinsically, but not exclusively, linked to pressure variations along the entire surface due to various factors such as the formation of longitudinal vortices, with particular emphasis on the nose shapes of the train - see figure 2a. These vortex sheets originate from the three-dimensional boundary layer and give rise to forces and moments of magnitude high enough to compromise the stability of the vehicle. Such action of forces and moments can lead to the lateral collapse of the train. Not less important is the formation of longitudinal vortices, as represented in figure 2b, after tests carried out at the IST *Instituto Superior Tcnico* in the light train in the belt region.

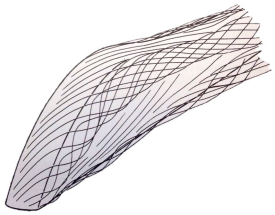

(a) Longitudinal vortices on the front section.

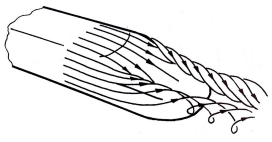

(b) Longitudinal vortices in the rear of the train.

Figure 2: Longitudinal vortices in the train [1].

Tree-dimensional boundary Layer The torsion of the boundary layer, which originates from a transverse pressure gradient, is defined as the local deviation of the limits lines with respect to the direction of the external flow – see figure 3 – which causes differences in velocity, either in the modulus or in the direction along the thickness of the boundary layer. The deviation of these lines is greater in the region next to the wall due to the necessity to be guaranteed the balance between the radial pressure gradient and the centrifugal force per unit volume - an inverse mechanism called the second kind [2]. The techniques of visualization of the flow near the surface, like the one that was used in this work, allow to observe these lines of limit current. These lines indicate the local direction of the flow near the wall. Due to the twisting of the boundary layer, the application of the visualization techniques of the boundary current lines only indicates the direction of the lines near the surface, not the direction taken by the external current lines. However, through the pattern of the current lines, zones can be identified where, by conservation of mass, separation of three-dimensional boundary layer, which are defined as places where distinct boundary current lines, converge to the same location, leaving the surface as a single current line [5] [2]. In figure 4 is shown a simplification of the convergence of current lines, which cause the separation of the boundary layer. The three-dimensional separation gives rise to the longitudinal vortices.

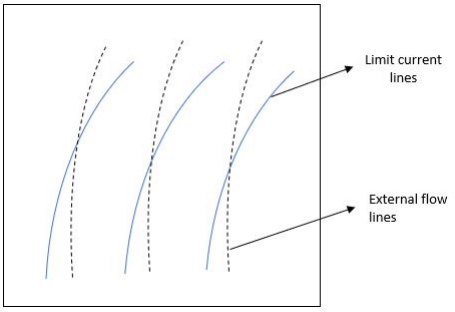

Figure 3: Deviation of lines outside the boundary layer and near the wall.

Suction Control The suction of the boundary layer takes advantage of the fact that the transverse component of the velocity - w' - is very close to the wall, where the flow velocity is lower compared to the main flow. Removal of this lower layer within the boundary layer may reduce the torsion effect and possibly prevent a separation of the three-dimensional boundary layer.

The train model was previously built in order to allow the application of this technique. As such, and given the exclusive interest in the treadmill of it, half the model is hollow. In this way it is puncture of small holes, or grooves - where suction is hole

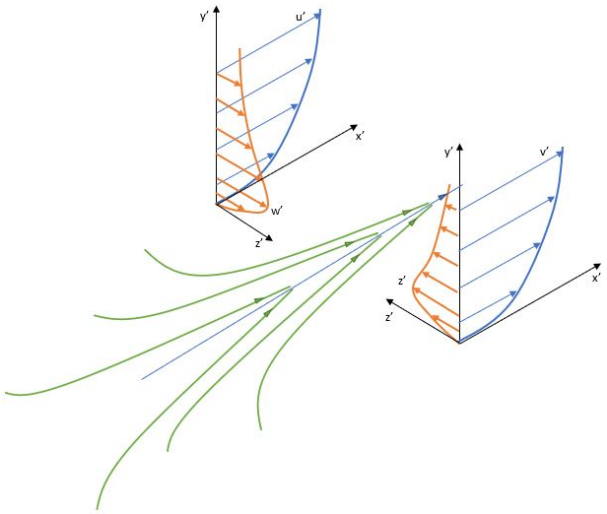

Figure 4: Simplified representation of the deviation in the flow, with the convergence of the current lines (green lines).

in the lower part of the train, to which the same air will be drained - see figure 5.

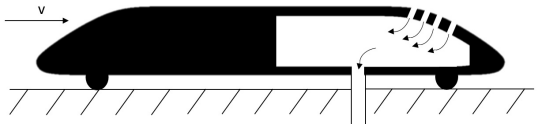

Figure 5: Simplified representation of suction control in the model.

4. Experimental tests

The model was fabricated from 100 mm thick extruded polystyrene plates, cut and machined in twenty-one slices by a CNC machine (*Computer Numerical Control*). Three aluminium tubes were used, which give flexural strength to the model, and guided the slices during assembly. White pigments were used and therefore the model was painted in matt black to increase the contrast. Ten layers of paint were applied, which succeeded the application of three thin layers of bitumen. Polishing was done with fine grit, until a smooth finish and without brush marks were obtained, so that they did not affect the visualization of the superficial cut lines.

Maximum thickness and velocity of the oil film An oil film of thickness ϵ is subject to the shear stress τ_w exerted by the main flow and its own weight as well as the reaction of the solid surface at the solid-liquid interface. The component of the weight orthogonal to the solid surface is absorbed by the compression of the same. The tangential component of the weight and the shear stress[4] are given by:

$$\tau_p = \rho \varepsilon g \cos(\theta) \tag{1}$$

$$\tau_w = C_f \frac{1}{2} \rho U_e^2 \tag{2}$$

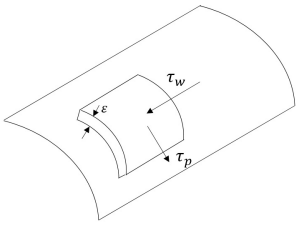

Figure 6: Representation of shear stresses applied to a fluid element on an inclined surface.

For a Reynolds number between 2×10^6 and 4×10^6 and considering $C_f = 0,0581 Re_x^{-\frac{1}{5}}$[4] and for the extreme case of a vertical wall ($\theta = 0$), maximizing τ_w with respect to τ_p, for the gravitational effect to be minimized, one obtains:

$$\tau_w \gg \rho_f \varepsilon g \tag{3}$$

From 3 and to:

$$\frac{\tau_w}{\tau_p} > 100 \tag{4}$$

For $\rho_f = 850$ kg/m^3, $\tau_w = 1{,}6$ Pa, from the equations 3 and 4:

$$\varepsilon < \frac{1,6}{850 \times 9,81 \times 100} \simeq 1,9 \mu m \tag{5}$$

This estimate of ε indicates the granulometry of the pigment.

Considering zero pressure gradient ($\frac{dp}{dx} = 0$), the velocity profile within the oil film is linear (Couette flow) and is given by:

$$u(y) = U_0 (\frac{y}{\varepsilon}) \tag{6}$$

Where U_0 is the velocity at the oil-air interface. The shear stress is uniform throughout the thickness ε:

$$\mu \frac{\partial u}{\partial y} = \tau_w \tag{7}$$

so:

$$U_0 = \frac{\tau_w}{\mu} \varepsilon \tag{8}$$

Using ε from 8, the velocity at the oil-air interface for different fluids are tabulated in the following table:

Elements	Velocity [mm/s]
Oil 10W40	1.45
Petrol	$9,4 \times 10^2$
Diesel fuel	$1,3 \times 10^2$
Kerosene	2×10^2
Propanol	$1,7 \times 10^2$
Gearbox oil	$7,6 \times 10^{-1}$
50% Oil + 50% Kerosene	$1,7 \times 10^{-1}$
80% Oil + 20% Kerosene	3.9

Table 1: Velocity of different fluids.

It is intended that the oil speed flow slowly to prevent splashing, although not excessively low, which could result in too slow. The table 1 suggests that mixtures of oil and kerosene can make the flow sufficiently slow, but not excessively.

5. Wind-tunnel and test procedure

The test facility is a closed-loop wind tunnel with an airtight test chamber of rectangular cross-section, of 1.50 m x 1.20 m where the wind is uniform and the turbulence intensity does not exceed 1%. The reference wind speed, V, is calculated from the dynamic pressure, measured at the entrance of the test chamber with a precision Betz type manometer with a resolution of 0.1 Pa, and the flow temperature. The fan control system is based on a frequency converter that allows the flow speed to be set and maintained[8].

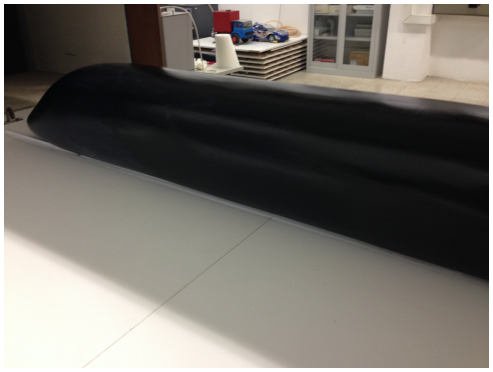

Figure 7: Model in wind tunnel.

Similarity between the model and prototype For practical reasons, it is sometimes difficult or even impossible to ensure that all relevant dimensionless numbers in the aerodynamic study are the same. In the case of the model it is not possible to ensure the same Reynolds number. However it is possible to perform tests at different Reynolds numbers, since at high Reynolds numbers the coefficient of drag is approximately constant.

The model of the train was raised at the rear to take into account the displacement thickness on the tunnel floor. The elevation was 5 mm because the growth rate of the predicted displacement thickness is 1.6 mm/mm

As shown in the figure 8 we have three types of speed profiles under the train:

- case A, represents the case of wind tunnel with moving floor with velocity equal to the velocity of the approach flow.

-Case B, also verified in the tunnel, the velocity profile displayed is due to the fact that the speed of the train and the speed of the ground are zero.

- Case C - The velocity profile represented is of the tests with the displacement thickness correction.

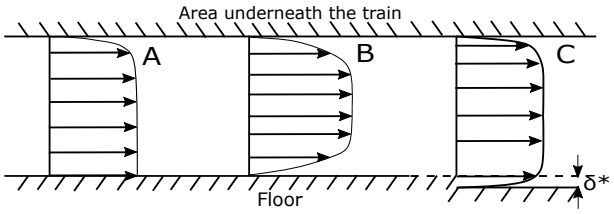

Figure 8: Velocity profiles under the train, for three situations. A - Real profile with referential in the line; B - Profile in the tunnel; C - Profile in the real case, with reference in the train.

Wind tunnel blockage effect The blocking effect can be neglected, since the local flow rate ratio with and without the model is 1.04, for a zero yaw angle. For a non-zero yaw angle, it continues to be neglected due to the sufficiently large distance from the train to the tunnel walls.

Angular deviation of a particle Considering a grain particle of a pigment immersed in an oil film, subject to the action of gravity — Weight P and the drag force — $\vec{D}$ —, schematized in 9.

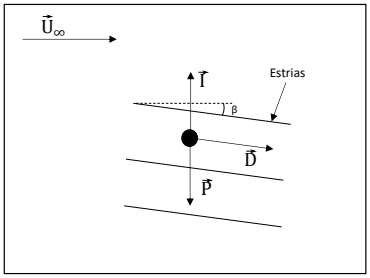

Figure 9: Grain dragged into the oil film subject to gravity.

In an unconfined environment:

$$\vec{P} = \frac{4}{3}\pi r^3 \rho_1 \vec{g} \tag{9}$$

and

$$\vec{D} \propto 6\pi\mu r\vec{V_r} \tag{10}$$

where ρ_1 is the density of the grain, $\vec{V_r}$ is the relative velocity and r is the particle radius.

To minimize the effect of gravity, we intend to:

$$\frac{|\vec{D}|}{|\vec{P}|} \gg 1 \tag{11}$$

Replacing the equations 9 and 10 into 11:

$$\frac{\mu\vec{V_r}}{\rho_1 g r^2} \gg 1 \tag{12}$$

From equation 12, we conclude that the smaller particles tend to follow the fluid with less influence of the gravitational force

Angular error Tests were performed to determine the maximum deviation of the lines of surface shear stresses - stretch marks - in relation to the horizontal, in the limiting case of a flat plate placed vertically. The tests were performed at three different velocity, calculated through the equation 13, from the measurements made with a liquid column gauges.

$$v = \sqrt{\frac{2\Delta p}{\rho_{ar}}} \tag{13}$$

whereΔp is the dynamic pressure, being calculated by:

$$\Delta p = \rho_{alcool} g \Delta h \tag{14}$$

where ρ_{alcool} is 850 kg/m^3 and Δh is the height difference between the static pressure tube and the dynamic pressure tube. In the table 2, Δl represents the length measured on the pressure gauge and, α the inclination of the pressure gauge. The vertical height is: $\Delta h = \Delta l\ sin(\alpha)$.

	Test 1	Test 2	Test 3
Δl [mm]	75,9	102	130
α [°]	36,7	36,7	36,7
Δh [mm]	45,3	60,9	77,7
Δp [Pa]	378,2	508,3	647,8
Velocity [m/s]	24,3	29,1	32,9
β [°]	9,7 ± 1,4	4,7 ± 0,9	3,8 ± 0.08

Table 2: Test speed and deviation from the horizontal of a stretch marks, in degrees - β. The angle α is the slope of the manometer.

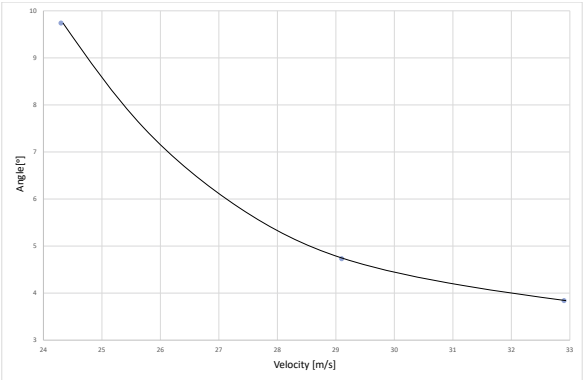

Figure 10: Angular error.

The graph suggests a hyperbolic function of the approach flow velocity. It is an expected result because $\tau_w \propto U_e^2$ once:

$$\tau_w = f(C_f, \rho, U_e^2) \tag{15}$$

where $C_f = f(Re)$ (considering Re approximately constant).

Striation formation mechanism The air flow over the oil film produces shear stress at the oil-air interface. Under the action of these shear forces, the oil is scattered on the surface decreasing its thickness. The particles accompany this movement. As the oil evaporates, the particles in suspension begin to settle and the process of formation of the striations begins. The deposition of grain on the surface constitutes an obstacle against which other grains successively collide. Some grains do not clash against those that are already deposited, but due to the thinning of the oil film, they will later deposit on the surface or beached in another grain.

The mixture of the oil film There is no formula in the literature that indicates the exact proportions

to be used. However, there are some suggestions available in [3], which were used to developed the visualization technique. It depends on several factors such as the speed of the flow, the surface, the components used, etc.

The technique was refined until a mixture was obtained that allowed a good visualization of stretch marks.

The pigment In order to try to solve the problem of reflectivity in the model, described in [7], as in some works of visualization of flows, was chosen a pigment that when excited with radiation incident in the ultraviolet range (UVA - black light) - $\lambda \in [315,400]$ nm, display a brightness in dark environment[6]. At first attempt was used a phosphorescent pigment GSS which consists of a very fine crystal of zinc sulphide doped with copper ($ZnS : Cu$). Their average particle size is 23 μm with a variance of 3 μm. The average particle size of titanium dioxide is 0,21 μm.

Phosphorescent pigment Several tests were performed to try to obtain stretch marks with the phosphorescent pigment. Tests were performed on horizontal flat plate and on the model of the train. The results obtained for the phosphorescent pigment were a homogeneous oil film, with streaks of difficult visualization - See figure 11. In the case of flat plate tests, it was further sought to change the thickness, ϵ, of the oil film, as well as to change only the amount of the dispersant of the blend - linseed oil.

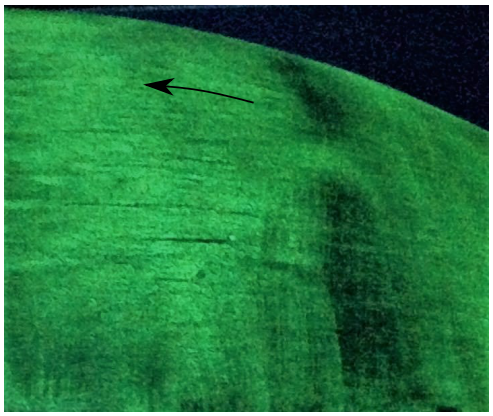

Figure 11: Homogeneous flow of phosphorescent pigment.

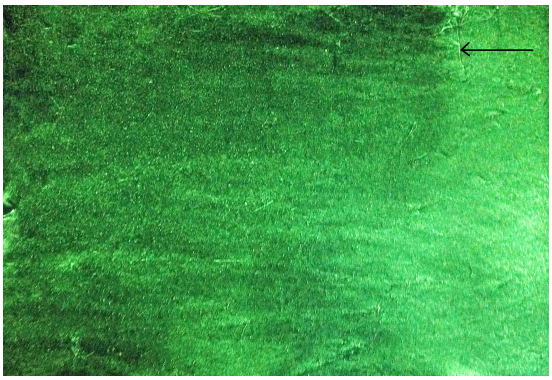

Figure 12: Flat plate flow of phosphorescent pigment.

Phosphorescent particle visualization To understand the non-formation of stretch marks with the use of phosphorescent pigment the phosphorescent pigment grains were seen under a microscope. These views were made with two resolutions – 10x and 50x. The result of a resolution of 50x is shown in figure 14. Particles of different sizes can be identified, whose measured size was between 3 μm and 26 μm. This difference in size, and the high size of some particles may explain the non-formation of stretch marks.

An observation of titanium dioxide with a resolution of 50x was also made. However the microscope used was designed for the visualization of phosphorescent and fluorescent particles and having a minimum size in the order of 1 μm, which prevented a good visualization of the titanium dioxide pigment.

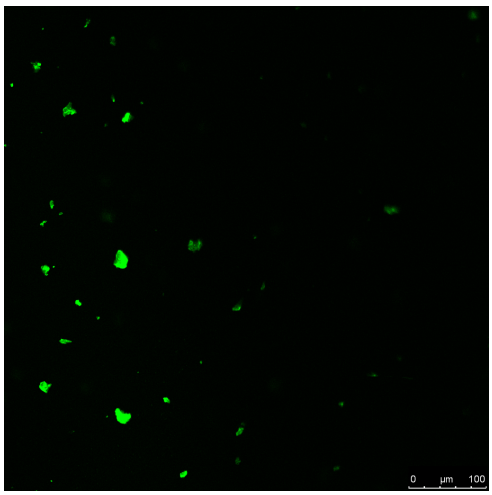

Figure 13: Visualisation in the microscope of the phosphorescent pigment with 10x resolution.

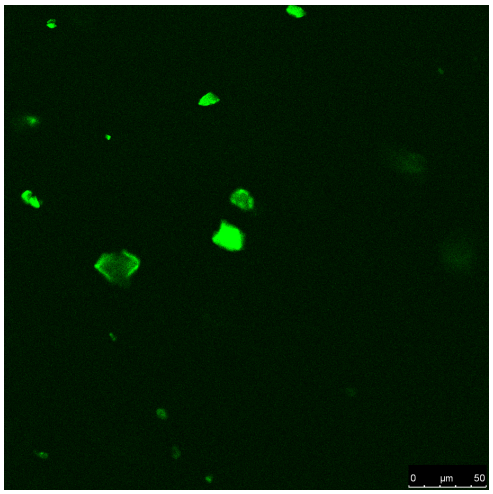

Figure 14: Visualisation in the microscope of the phosphorescent pigment with 50x resolution.

Complementary tests Were done some more tests with different pigments: fluorescent dye and spheres of silica with dye. Both of the pigments are supplied by *Centro de Qumica-Fsica Molecular do IST*.

The figures 15 and 16 shows the results of the flow with fluorescent dye with linseed oil and with silica particles dyed with fluorescent dye. Other tests were performed without linseed oil, and adding more oil and kerosene. The results were a much more homogenous aspect for all cases, without any visible striation.

In the case of silica spheres the appearance of visible grains was observed - see A and B in the figure 16.

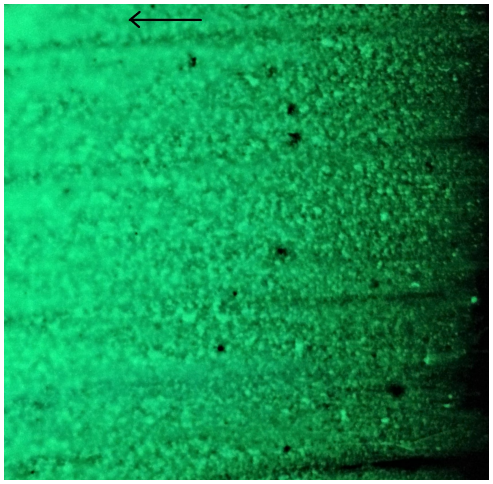

Figure 15: Fluorescent dye with linseed oil.

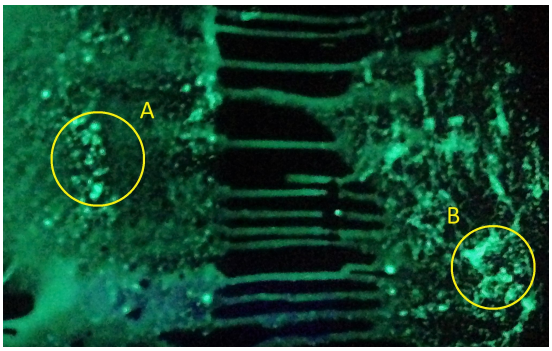

Figure 16: Flow with silica particles dyed with fluorescent dye.

6. Results

Tests were performed for null yaw angle and with a yaw angle of 12 and 20 degrees. The choice of angles is related to the tests performed in [7], to allow the comparison of the results obtained. To obtain the photographic records a camera was used *Sony dsc-w550*.

Null yaw angle The tests were performed simultaneously on the front and rear sections of the model, trying to find zones of convergence of the superficial shear stress lines. The tests were performed at speeds in the order of 27 m/s.

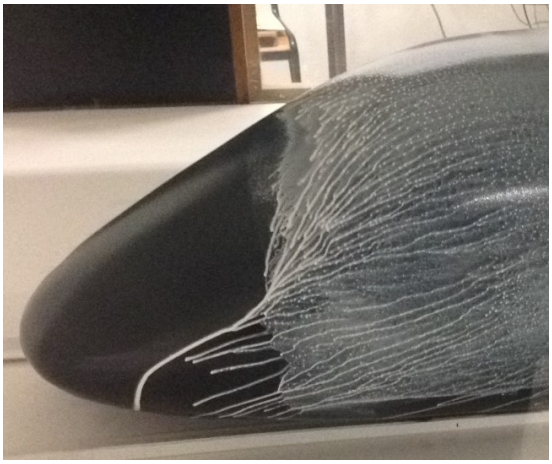

Figure 17: Appearing of the separation region before in an initial phase.

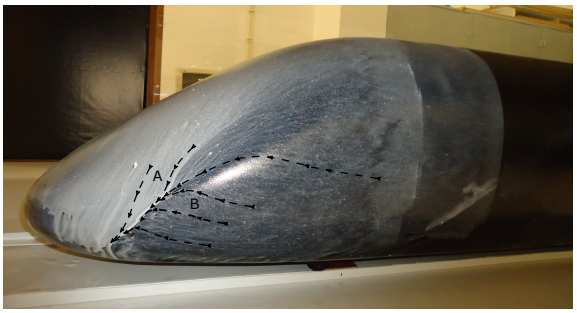

Figure 18: Convergence of shear stress lines at the rear of the model.

From the observations of the striations, in the figure 18, it is verified that the upper flow is diverted to the side - lines A of the figure 18 -, and simultaneously, the lower flow is deflected upwards - lines B of the figure 18. The striations converge giving rise to a zone of separation. The region of convergence and separation of the boundary layer is displaced in relation to the exact location due to the gravitational effect. However, the deviation of the striations is small when the oil film is already stretched, especially since the surface of the model is not vertical in this zone.

At a later stage in the stretching of the oil one already notices the convergence of the boundary current lines, locating the separation of a vortex sheet.

The twisting of the boundary layer leads to the deviation of the current lines.

Tests with non-zero yaw angles The figure 19 represents the assembly scheme in plan of the model for non-zero yaw angles – θ. The tests were performed with an approximate flow velocity also in the order of 27 m/s.

For security two wires were placed to hold the model laterally. In all tests the model was also secured longitudinally by a thin wire.

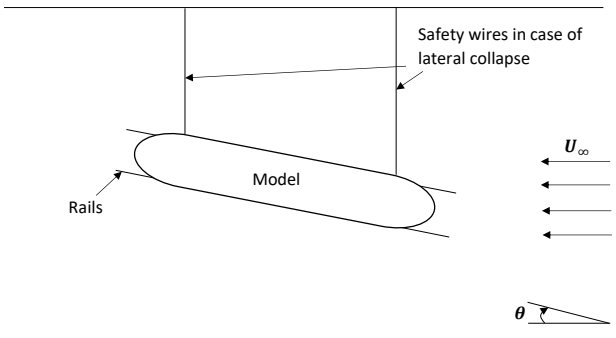

Figure 19: Schematic representation of the assembly for tests with non-zero yaw angle.

12 degree yaw angle In the front region of the train the appearance of a separation line in the lower zone of the train was observed, as predicted by [7]. In the figure **??**, the striations are not yet formed next to the seperation of this vortex but it is already noted that the upward velocity component in zone A is sufficient to counteract gravity, where exists the generation of a longitudinal vortex, which was verified using the wool method. In region A of the figure 20 no oil film was applied, however it is evident that the flow is upward in the direction of the white line, above A.

On the right side of the model (leeward) a slight downward displacement of the line of convergence was observed with respect to the test with a zero yaw angle, as well as a significant increase in the extent of the same, visible on the white line in 22. The picture of the figure 21 was taken at a time when an oil film was still stretched in some regions.

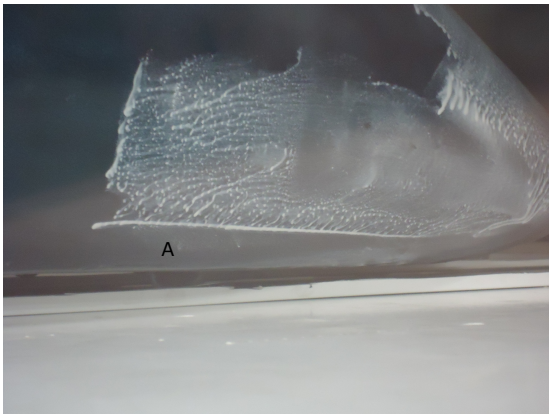

Figure 20: Formation of longitudinal vortex in the front and lower section of the model.

Convergence of shear stress lines:

Figure 21: Separation zone in the rear of the model with indication of the local direction of surface current lines.

Figure 22: Extension of separation in the rear region.

20 degree yaw angle In earlier experiments[7] with this geometry, with a smaller model, it was verified the appearance of longitudinal vortices to develop from the nose of the train at a yaw angle of 18°. But in the present model these vortices were not detected. This model has a Reynolds number 18% higher than the previous model and that may explain the non-appearance of the longitudinal vortices in this region; with the increase of Reynolds number it was not necessary to force the transition of the boundary layer. In the smaller model the laminar flow fraction was significant throughout the length of the nose, to the extent that it was necessary to force the transition of the boundary layer near the stagnation point.

Areas with large accumulation of oil were observed. These zones were analyzed successively, concentrating only the oil film in those regions. They are regions where the model has suffered a deformation. For smaller angles of yaw, these imperfections have no consequences but, at 20°, they cause septation lines – see zone A of the figure 23.

The velocity of the flow outside the boundary layer varies greatly from point to point in the model and it was not possible to dose the proportions of the appropriate oil, pigment and linseed oil simultaneously to all regions. At the rear of the model the appearance of stretch marks was more limited because for this yaw angle, the observed region is now dominated by low speeds. Therefore, there are few areas with the oil film fully stretched, the oil accumulation being high. For this reason it is not clear the region of convergence of the lines, however the direct observation evidences two of these lines, S and T, in the figure 24.

By successively analyzing the various zones, it is concluded that up to 20° of yaw angle, the upper longitudinal vortex was non-existent or incipient. This means that the pressure distribution is relatively symmetrical to windward and leeward and therefore the resulting lateral force and the aerodynamic dropping moment are small. In zone B of figure 23, the oil film is drawn in a small region. In this region, the boundary lines are perfectly horizontal, showing no convergence. The pattern appears to be similar across all other areas of the nose, except at a very low elevation (about 10% of model height).

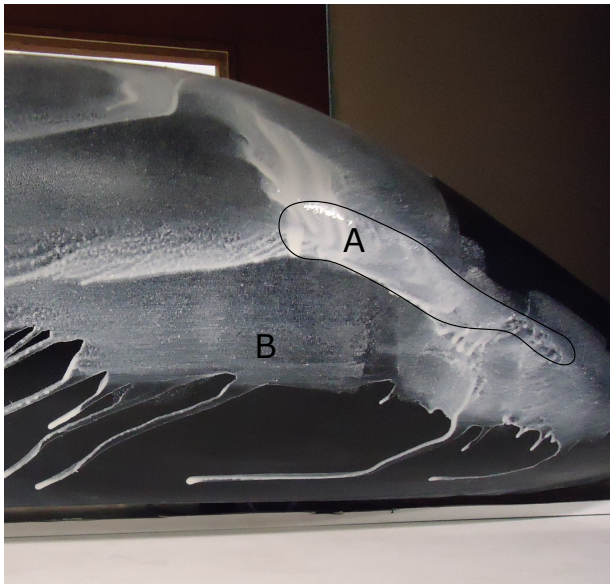

Figure 23: Separations due to geometric imperfections of the model.

Figure 24: Regions where there appears to be convergence of surface shear stress lines.

Application of the suction layer technique One of the objectives of this research was to obtain indications to improve the aerodynamic performance of this vehicle. In the tail of the train, the longitudinal separations depend on the twist of the boundary layer – as represented in the figure 25a. This figure suggests that it would be of great interest to suction the boundary layer in this zone. It is

known that the torsion of the boundary layer is concentrated in the region of the wall (about 10-15% of the thickness of the boundary layer) and therefore is the approximate thickness which should be removed. This intervention would shift the separation line to the longitudinal plane of the symmetry of the train, with the advantage of increasing pressure recovery at the rear and, above all, reducing lateral force at the rear of the train.

Up to about 20% of the yaw angle, the only longitudinal separation from the nose is the low dimension (10% of the height), thus not significantly influencing the lateral force, the overturning moment and the production of aerodynamic noise with impact outside the rails.

However, for this very high yaw angle, a longitudinal vortex was formed below the curve between the side wall and the roof, approximately 60% of the height, from about half of the train.

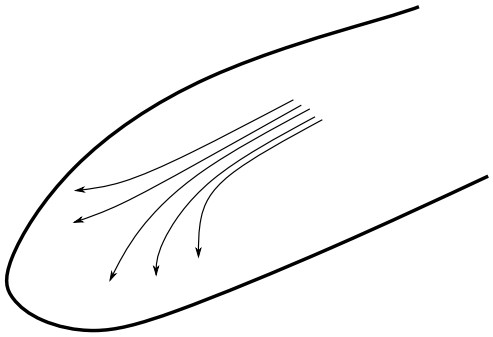

(a) Limit current lines at the back of the train.

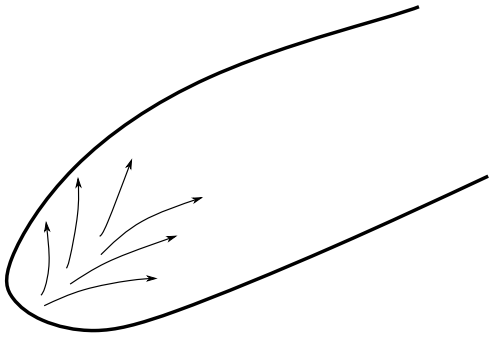

(b) Limit current lines on the nose of the train.

Figure 25: Limit current lines.

7. Conclusions

The investigation of this work allowed to conclude that the implementation of the oil film method requires sensitivity in the dosage of the components used in the mixture, as well as the need to guarantee a thickness of the oil film in the order of 1 μm, uniformly spread over the surface, due to the gravitic effects.

Research on the pigments used in the oil mixture revealed the importance of the size of their grains for the understanding of the mechanism of formation of the stretch marks.

In the tests carried out in the front and rear of the train, zones of convergence of the surface tension lines were identified. These lines are indicative of three-dimensional boundary layer separation. Locations for air extraction were suggested, based on the location of these lines.

In the twist angle test of 20° the absence of the upper longitudinal vortex in the nose of the train suggests that the Reynolds number plays a decisive role in the accuracy of the results obtained. The observations made to the surface shear stress lines allowed to determine that an advantageous place for the extraction of fluid from the boundary layer would be in the tail of the train, namely in the central and upper zone.

"The geometry of this model shows a well developed aerodynamic design, since the train is so fuselated that only the friction between the wheels of the train and the floor of the tunnel was sufficient to guarantee that the model was not dragged by the flow.

References

[1] J. M. C.S Andr. *Transporte Interurbano em Portugal - 2 Volumes*. IST - Instituto Superior Tcnico, 2008.

[2] V. De Brederode. *Aerodinmica incompressvel: Fundamentos*. IST - Instituto Superior Tcnico, 2014.

[3] O. D. T. De L'Atlantique. Flow visualization in wind tunnels using indicators. AGARD, 1962.

[4] L. Eça. Clculo de parmetros integrais de camada limite em gradiente de presso nulo. 2008.

[5] E. Maskell. Flow separation in three dimensions. Technical report, 1955.

[6] V. Mosharov, A. Orlov, and V. Radchenko. New approach to surface oil-flow visualization. In *Instrumentation in Aerospace Simulation Facilities, 2005. iciasf'05. 21st International Congress on*, pages 176–180. IEEE, 2005.

[7] I. d. M. B. Pereira. *Aerodinmica de comboios de alta velocidade*. Universidade de Lisboa, Instituto Superior Tcnico (Lisboa), 2014.

[8] D. C. Vaz, R. A. Almeida, E. Didier, A. P. Urgueira, and A. J. Borges. Improving the aerodynamic performance of vila-real bridge deck-section. *Journal of Wind Engineering and Industrial Aerodynamics*, 156:72–83, 2016.